ISSN: 0067-2904

Synthesis, Characterization and Application of [PVA-g-P (AAm-co-MBA)] /Fe_3O_4/ DES- Based Magnetic Composite for Rhodamine B Dye Adsorption

Zain Al-Abideen Amer Jameel, Faiq F. Karam*
Department of Chemical, College for Sciences, University Al-Qadisiyah, Iraq.

Received: 20/5/2025 Accepted: 3/ 9/2025 Published: 30/ 8/2026

ABSTRACT

The research reports the synthesis, characterization, and application of a unique magnetic polymeric composite, a polyvinyl alcohol-grafted poly (acrylamide-co-methylenebisacrylamide) incorporated with iron oxide nanoparticles and deep eutectic solvents [PVA-g-P (AAm-co-MBA)]/Fe_3O_4/DES. The composite comprises polyvinyl alcohol-grafted poly (acrylamide-co-methylenebisacrylamide) integrated with iron oxide nanoparticles and deep eutectic solvents. The main aim is to create an effective, environmentally sustainable adsorbent for the removal of Rhodamine B (RB), a toxic cationic dye, from water solutions. DES was created using choline chloride with urea (1:2 ratios), and combined with PVA, acrylamide, MBA, and Fe_3O_4 nanoparticles to construct a hydrogel- based magnet nanocomposite. Diffraction of X- Rays (XRD), infrared spectroscopy with the Fourier transform (FTIR), and field emission scanning electron microscopy (FESEM) validated the hydrogels amorphous and permeable character, as well as the successful integration of magnetized nanoparticles and adsorption friendly functional groups. Batch adsorption tests were carried out to determine the influence of different factors such as contact duration, pH, temperature, adsorbent dose, and ionic strength on RB removal effectiveness. The composite exhibited rapid adsorption, reaching equilibrium in approximately one hour and achieving a maximum removal efficiency of 68.3% under optimal circumstances. The adsorption process had pseudo-second-order kinetics and best suited the Langmuir isotherm model, implying multilayer adsorption on a heterogeneous surface. Thermodynamic investigations showed that RB adsorption was exothermic with a negative enthalpy change ($\Delta H°$ = -6.837 kJ/mol). The composite was likewise sensitive to ionic strength and pH, with optimal adsorption occurring at pH 6. The study supports the composite's significant potential for wastewater treatment applications due to its reusable nature, magnetic separability, and ecologically benign production method.

Keywords: Fe_3O_4 nanoparticals, (DES), PVA, water treatment, polymer nanocomposite, Rhodamine B, dye removal, Adsorption

تخليق وتوصيف وتطبيق مركب مغناطيسي قائم على [PVA–g–P (AAm–co–MBA)]/Fe_3O_4/DES لأستخلاص وامتزاز صبغة الرودامين B

* Email: faiq.karam@qu.edu.iq

زين العابدين عامر جميل ، فائق كرم*

قسم الكيمياء، كلية العلوم، جامعة القادسية

الخلاصة

يُبلغ هذا البحث عن تحضير وتوصيف وتطبيق مركب بوليمري مغناطيسي فريد، وهو بولي فينيل الكحول المطعّم على بولي (أكريلاميد-كو-ميثيلين بيس أكريلاميد) المدمج مع جسيمات أوكسيد الحديد النانوية والمذيبات الأيونية العميقة [PVA-g-P(AAm-co-MBA)]/Fe_3O_4/DES. يتكون المركب من بولي فينيل الكحول المطعّم على بولي (أكريلاميد-كو-ميثيلين بيس أكريلاميد) المدمج مع جسيمات أوكسيد الحديد النانوية والمذيبات الأيونية العميقة. الهدف الرئيسي هو إنشاء مادة ماصّة فعّالة وصديقة للبيئة لإزالة صبغة الرودامين B (RB)، وهي صبغة كاتيونية سامة، من المحاليل المائية. تم إنشاء المذيب الأيوني العميق باستخدام كلوريد الكولين مع اليوريا بنسبة (1:2)، ودمجه مع PVA والأكريلاميد وMBA وجسيمات Fe_3O_4 النانوية لتكوين هيدروجيل نانوي مغناطيسي. وقد أكّد حيود الأشعة السينية (XRD) والمطيافية تحت الحمراء بتحويل فوريه (FTIR) والمجهر الإلكتروني الماسح بانبعاث المجال (FESEM) الطبيعة غير المتبلورة والمساميّة للهيدروجيل، بالإضافة إلى الدمج الناجح للجسيمات النانوية المغناطيسية والمجاميع الوظيفية الملائمة للامتزاز. أُجريت تجارب الامتزاز بالدفعة لتحديد تأثير العوامل المختلفة مثل مدة التلامس ودرجة الحموضة ودرجة الحرارة وجرعة الماصّ والشدّة الأيونية على كفاءة إزالة RB. وأظهر المركب امتزازاً سريعاً، حيث وصل إلى حالة الاتزان في حوالي ساعة واحدة وحقق أقصى كفاءة إزالة بلغت 68.3% تحت الظروف المثلى. وقد أظهرت عملية الامتزاز حركية من الدرجة الكاذبة الثانية وتوافقت بشكل أفضل مع نموذج متساوي الامتزاز لانكماير، مما يشير إلى حدوث امتزاز متعدد الطبقات على سطح غير متجانس. وأظهرت الدراسات الثرموديناميكية أن امتزاز RB كان طارداً للحرارة مع تغير سلبي في المحتوى الحراري (ΔH° = −6.837 kJ/mol). كما كان المركب حساساً للشدّة الأيونية ودرجة الحموضة، حيث حدث الامتزاز الأمثل عند درجة حموضة مقدارها 6. وتدعم هذه الدراسة الإمكانات الكبيرة للمركب في تطبيقات معالجة مياه الصرف بسبب قابليته لإعادة الاستخدام وسهولة فصله مغناطيسياً وطريقة تحضيره الصديقة للبيئة.

1. Introduction.

The growth of human populations and increased activity have led to rising water pollution rates. Polluted water is an important environmental issue concern caused by the release of polluted effluents from many anthropogenic sources[1]. Industries such as leather tanning, petroleum refining, paint, textiles, heavy metals, wood processing, and dye manufacture contribute significantly of water pollution[2]. Although both cationic and anionic dyes are classified as "dyes," cationic dyes regarded as more dangerous than anionic dyes due to their electrostatic interactions with negatively charged cellular constituents, which promote membrane infiltration and cellular harm. Furthermore, wastewater from dyeing processes contains carcinogenic, mutagenic, and allergenic qualities posing serious threats to both receiving water bodies and the surrounding environment. [3]. Polluted wastewater must be treated to avoid environmental damage. There are several treatment options accessible, including biological, physiochemical, lipid separating, the ozone layer and further oxidation, and integrated methods. Because dye waste water is poorly biodegradable, conventional biological removal approaches are unsuccessful. Physical or chemical approaches are frequently utilized to address this issue. However, due to costs and disposal issues, these devices cannot process all forms of dyes water waste [4]. The adsorption was a common means of eliminating pollutants due to it's cheap, efficient, and easy to use[5]. The adsorption method may reuse and recycle an adsorbent in an economical, efficient, and easy manner. Adsorption, like coagulation and activated sludge, generates secondary trash following treatment. The adsorbent's adsorbed capability and reusability are important in this context.

The product's utility is enhanced by its abundance, environmentally friendly structure, and low production cost. The effectiveness of the Adsorption technique is strongly impacted by the adsorbent's surface chemical composition. Chemical modifications can increase the number of active sites and potential groups with function[6]. The adsorption is influenced by numerous process parameters, such as dosage of adsorbent, pH, temperature, ionic strength, and adsorption material properties [7]. Rhodamine B, (RB) is a synthetic colorant utilized in the manufacture of dyes lasers, stamp pad inks, fireworks, carbon sheets, and ballpoint pens. Figure 1, displays the substance's structure is N-[9-(2-carboxyphenyl)-6-(diethylamino)-3H-xanthen-3-ylidene]-N-ethylethanaminium[8]. Due to its non-destructible character as inherent stability in structure, RB was later classified as toxic to neurons, cancer-causing, as well as capable of producing respiratory tract infections[9]. RB is a cationic dye dissolved in water, an amorphous pigment that belongs in the xanthene dye category C.I number: 45170 and λmax = 554 nm for RB dye. Its distinctive photophysical properties render it suitable as a water transporter florescent dye[10]. Effective removal of RB from water and wastewater is crucial. Previous research has investigated the removal of Rhodamine B dye using advanced adsorbents such as Fe_3O_4@ZIF-8, with adsorption capacities reaching 647.5 mg/g. Hybrid polymer hydrogels are highly effective in removing RhB protein due to their porous structure and functional groups [11].

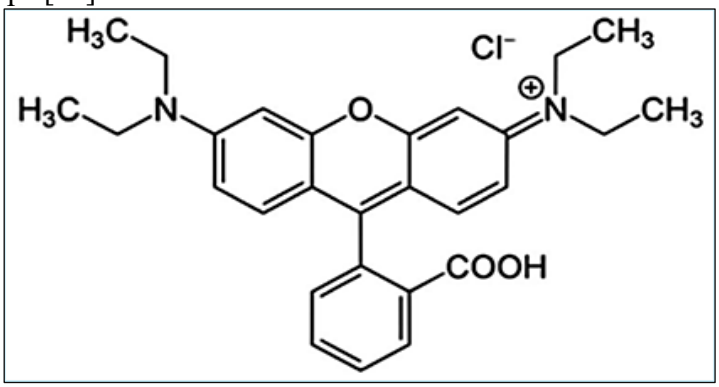

Figure 1: Composition of RB[12].

Deep eutectic solvents (DESs), a kind of ionic liquid (IL), are green solvents with many components that may produce eutectic mixtures by hydrogen bonding. These materials have unique features such as low melting point, low volatility and vapor pressure, good thermal stability, high solubility, and adjustable selectivity and hydrophobicity. These characteristics lead to them being better extractors than typical organic solvents that are used in extraction techniques [13]. During 2003 - 2020, there was a 50-folds rise in the total number of articles on the combination of choline chloride and urea at a 1:2 mol ratio (ChCl:U, also referred to as relines)[14]. ChCl:U is a type III deep eutectic system (DES), a liquid material formed by mixing an ammonium, phosphonium, or sulfonium salts and a tiny organic molecules that functions as a hydrogen bond donors (HBD)[15]. hydrogen bond acceptors facilitate charge delocalization across species, inducing a pronounced melting point depression in the combined system, significantly deeper than that observed in the individual components or an ideal mixture [16]. Magnetic DES (MDES) is an emerging class of DES which is gaining popularity in research. Initial studies on MDES concentrated on production and fundamental investigations, although its paramagnetic properties have prompted novel magnet- based approaches for analyzing chemicals [17]. Magnetic properties make MDES useful in separation techniques such as extraction, microextraction, absorption, and adsorption. They can speed up and streamline processes, reducing the number of steps required. This study aims to synthesis and characterize an eco-friendly magnetic composite composed of [PVA-g-P(AAm-co-MBA)]/Fe_3O_4 integrated with deep eutectic solvents (DES) and to assess its

efficacy as a high-performance adsorbent for the extraction and removal of Rhodamine B dye from aqueous solutions

2. Experimental

2.1. Materials

Choline chloride (purity 99.9) (Germany), Urea (purity 99.9) (UK), PVA (purity 98.0) (China), Acrylamide (purity99.0) (China.G.F.T), potassium persulfate (KPS) (purity 98.0) (Sigma-Aldrich), N, N-methylenebiascrylamide (MBA) (purity 99.0) (India, Thomas Baker), Fe_3O_4 Nanoparticles (purity 99.9) (Sigma-Aldrich), HCl (purity 36.0) NaOH (purity 99.9) (Pancreac Spanish), calcium carbonate (purity 98.5) (Fluka), with sodium chloride (purity 99.0) (Alpha Chemika). Rhodamine B (China) and M.wt = 479.02. All experimental procedures were initiated using distilled water.

2.2. Instruments

The material was analyzed using X-ray diffraction (XRD) on Analytic equipment from the Netherlands. Surface morphology was examined with a microscope with scanning electrons (SEM) type DME-95-50E. In addition, UV-Vis spectrophotometer, was used, and the functional groups present in the composites were identified through Infrared Fourier transform (FTIR) spectrum obtained with a Perkin Elmer device. A Brook Haven 90+ model from the United States.

2.3. Synthesis of adsorbent

2.3.1. Synthesis of DES (choline chloride + Urea) and PVA

Initially, 2.00 g of polyvinyl alcohol (PVA) was dissolved in 60 mL of distilled water using continuous magnetic stirring at 80°C until a clear and uniform solution was formed, indicating that the polymer had completely dissolved. Following that, a deep eutectic solvent (DES) was created by combining choline chloride (chcl) with urea in a molar ratio of 1:2. The mixture was placed in a flask with a magnetic stir bar and heated in a water bath at 70°C for 20 min with continuous stirring at 600 rpm until homogeneous. A homogeneous DES solutions was created[18]. Finally, the produced DES was mixed with the previously dissolved PVA solution under regulated temperature and stirring conditions to get a homogeneous mixture.

2.3.2. Synthesis of MDES Iron oxide nanoparticles / PVA (choline chloride + Urea).

To prepare the quaternary complex (MDES), 0.05 g of iron oxide nanoparticles (Fe_3O_4) was dissolved in a deep eutectic solvents (DES/PVA) solution and ultrasonically treated for 1 hour to ensure complete distribution and complicated construction.

2.3.3. Polymer synthesis [PVA-g-P (AAM-co-MBA)]/Fe_3O_4/DES.

Following cooling, 2 g of acrylamide (AAm) was dissolved in the MDES solution via continuous magnetic stirring until complete dissolution was achieved. In a second step, 0.1 g of N, N-methylenebisacrylamide was dissolved in 2 mL of distilled water and added to MDES/PVA -AAm combination. Nitrogen gas was supplied to the system to remove oxygen dissolved and avoid early polymers. Following that, 0.1 g potassium persulfate (KPS) was added to the reaction mixture while continuously whirling to achieve even distribution. The polymer formation method started with moving the mixture to an experiment tube and soaking it in a 70ºC water bath for an hour. Following polymerization, the hydrogel was thoroughly washed with distilled water to eliminate any monomers that did not react or residual impurities as shown in figure 2. The washed materials were finally dried in a

convection dryer with temperature varying between (60-80) ºC, lastly, a dried polymers was used to adsorbed Rhodamine B pigment from water-based solutions [11].

Figure 2: Polymer synthesis [PVA-g-P (AAM-co-MBA)]/Fe_3O_4/DES

2.4 Adsorption solution

Rhodamine B solution was generated by combining 0.01 g of the color in 650 mL (15 ppm) of distilled water. The acidity of the solution was changed using 0.1 M HCl or 0.1 M of NaOH.

2.4.1. Adsorption experiments.

The experiment was conducted in a 250 mL laboratory beaker with a mechanical vibrator revolving at 150 rpm until temperature equilibrium was reached at 25°C. The mass effect was evaluated by systematically removing particles from the adsorbent surface, with incremental increases from 0.01 to 0.1 g. The time effect was determined by measuring the adsorbent surface at different time points and applications. The implications of acidity were examined at pH levels 4, 6, 8, 10, and 12 by using a pH meter and pH indicator paper. Both salts, NaCl and $CaCO_3$, were employed in quantities that varied from 0.001 to 0.05 g to evaluate the impact of these ions on the surface [19]. A UV-Vis spectrophotometer was used to measure absorption at an effective wavelength of 554 nm and a concentration 15 ppm, the quantity of adsorbent was estimated using equation (1):

$$Qe = \frac{(Co - Ce)}{W} \times V \quad \ldots\ldots. (1)$$

Where W indicates the amount of [PVA-g-P (AAm-co-MBA)]/Fe_3O_4/DES used (g), V is the total volume of solution (L), and Co and Ce are the original and equilibrium RB dye concentration (mg/L). The procedure that calculating the proportion of Rhodamine B removed was given by Eq (2):

$$\text{Removal } (\%) = \frac{(Co - Ce)}{Co} \times 100 \quad \ldots\ldots. (2)$$

To determine the equilibrium concentration (Ce), a dye solution with a specified initial concentration (C_o) of 15 ppm is prepared. 10 mL of the dye concentration is added to exactly 0.01 g of adsorbent in a flask. The mixture is then stirred for a predetermined 60 minutes at 25°C and pH 6 until equilibrium is reached. The liquid is then centrifuged to isolate the solid adsorbent. The remaining dye concentration in the clear solution is measured using a UV-Vis spectrophotometer at the dye peak wavelength of 554 nm. The absorbance value is subsequently converted to the actual concentration using a calibration curve, and this final value is referred to as the Ce.

2.4.2. Adsorption isotherm

Adsorption isotherms are useful for understanding the interaction between the adsorption and surface areas, in addition to determining the ability to adsorb. They offer information on the quantity of levels that accumulate on the adsorbent outside, which can be interpreted as only one layer or a multilayered. Equations 3, 4 as well and 5 demonstrate this link [20].

Adsorption isotherm studies were carried out to investigate the interaction of Rhodamine B (RB) dye with the [PVA-g-P(AAm-co-MBA)]/Fe_3O_4/DES composite magnetic sorbent under equilibrium conditions. A series of batch experiments were performed by varying, the dye concentration (15) ppm at a constant sorbent dosage, temperature (25 °C), and pH 6. The samples were stirred in a thermocycler at 150 rpm for sufficient contact time to ensure equilibrium. After the solutions settled, they were spun in a centrifuge, and the leftover dye amounts were checked with a UV-Vis spectrometer at the peak absorption wavelength of RB dye (λmax = 554 nm). The amount of dye adsorbed at equilibrium (Q_e, mg/g) was calculated using eq.1:

Langmuir: $$\frac{Ce}{Qe} = \frac{1}{Qm} Ce + 1/Qm .K_L \quad \text{……. (3)}$$

Ce: Equilibrium concentration of the adsorbate (mg/L) Qe: Amount of adsorbate adsorbed at equilibrium (mg/g)

Qm: Maximum adsorption capacity (mg/g) K_L: Langmuir constant (L/mg)

Freundlich: $$\log Qe = \log K_F + \frac{1}{n} \log Ce \quad \text{……. (4)}$$

KF: Freundlich constant indicating adsorption capacity

1/n: Heterogeneity factor

Temkin: $$Qe = \frac{RT}{b} \ln K_T + \frac{RT}{b} \ln Ce \quad \text{……. (5)}$$

R: Universal gas constant (8.314 J/mol·K)

T: Absolute temperature (K)

b: Temkin constant related to the heat of adsorption (J/mol)

K_T: Temkin equilibrium binding constant (L/g)

, and Temkin isotherm constant B_T (J/mol) can be calculated using the following equation:

$$B_T = \frac{RT}{b} \quad \text{……. (6)}$$

2.4.3. Adsorption kinetics.

Kinetic experiments were performed under optimized conditions to investigate the interaction of Rhodamine B (RB) dye adsorbs with the [PVA-g-P (AAm-co-MBA)]/Fe_3O_4/DES magnetic composite. A specific amount of the composite adsorbent was added to several 100 mL solutions of RB dye, which had an initial concentration of 15 mg/L and a pH of 6. The mixtures were agitated at a constant temperature of 25°C using a thermostatic orbital shaker set at 150 rpm. At set times (between 5 and 120 minutes), samples were taken, spun in a centrifuge, and the liquid on top was tested with a UV–Vis spectrophotometer at 554 nm to find out how much dye was left. The amount of dye adsorbed at time t, denoted as q_t (mg/g), was calculated using:

$$q_t = \frac{(Co - Ct)}{m} . V$$

C_0 is the initial dye concentration (mg/L), C_t is the dye concentration at time t,

V is the volume of the dye solution (L), m is the mass of the adsorbent (g).

Equations (6, 7) show this in addition provides details about the process of adsorption and pathways, influences the adsorbed percentage, and dictates the length of time required to reach the adsorption process's balance conditions.

Pseudo first order: $$\log (q_e - q_t) = \log q_e – k_1/2.303\ t \quad \text{……. (7)}$$

Pseudo second order: $$t/q_t = 1/k_2\ q_e^2 + 1/q_e\ t \quad \text{……. (8)}$$

3. Results and discussion

3.1. X-ray diffraction (XRD) For [PVA-g-P (AAm-co-MBA)]/Fe_3O_4/DES.

Figure 3, shows the X-ray diffraction (XRD) pattern of the hydrogel composite noticeable wide hump centered at 20° in the 2θ range. This characteristic clearly indicates that the material is primarily amorphous. The absence of strong, clear diffraction peak shapes across the whole spectrum indicates a lack of distant crystal structure. The absence of strong, well

defined diffraction peaks over the whole spectrum demonstrates the lack of long-range crystalline organization, which is prevalent in soft, polymeric hydrogels or composite systems including deep eutectic solvent (DES) and organic matrices. The large peak at 20° is due to the semi-crystalline structure of polyvinyl alcohol (PVA), which in its pure form normally shows a distinctive (101) reflection about 19.5-20.2°. However, in this particular hydrogel matrix, the normally ordered crystalline domains of PVA undergo substantial structural disturbance. This is most likely due to substantial hydrogen bonding and intermolecular interactions between PVA and other included components, including acrylamide, the crosslinking agent MBA (N, N,-methlyenebisacrylamide), and the eutectic solvent composed of urea and choline chloride. These interactions disrupt the normal arrangement of PVA chains and decrease the overall degree of crystallinity, producing a wide, less strong diffraction pattern. Furthermore, the polymeric hydrogel network produced by acrylamide and MBA is essentially amorphous. These crosslinked polyacrylamide chains do not have periodic atomic ordering and provide no strong diffraction patterns in XRD [21]. Their existence, however, contributes to the pattern's vast, featureless background. The eutectic combination of urea and choline chloride, which serves as a plasticizing or structural modification medium in the system, is likewise totally amorphous. Because deep eutectic fluids form via hydrogen bonding rather than ionic or crystalline lattices, they lack typical diffraction peaks, enhancing the wide amorphous signal in the low-angle area of the XRD. Despite being crystalline in bulk, Fe_3O_4 nanoparticles lack identifiable diffraction peaks in this spectrum. Magnetite has significant reflections at 30.1°, 35.5°, 43.1°, 53.4°, 57.0°, and 62.6° (20), indicating its spinel structure. Their absence in this pattern might be explained by a variety of variables. The presence of Fe_3O_4 particles in ultrafine, nanoscale form (usually <10 nm) reduces the intensity and sharpness of diffraction peaks due to decreased scattering coherence. Second, these nanoparticles are most likely contained or well-distributed inside the thick, crosslinked hydrogel matrix, particularly within the PVA and polyacrylamide network, limiting their surface crystallinity and perhaps masking their existence in XRD [22]. The crystallite size (D) derived from X-ray diffraction using the Scherrer equation is D = 9.25 nm.

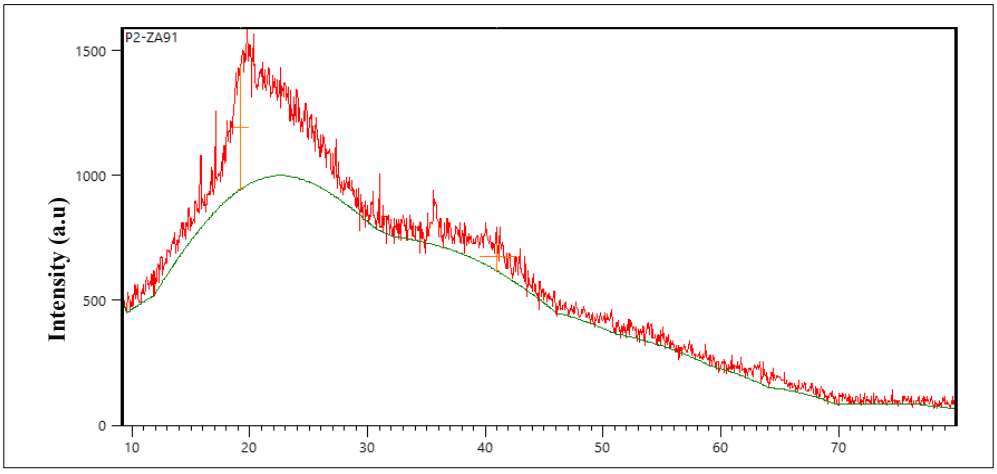

Figure 3: XRD diffraction patterns of [PVA-g-P (AAm-co-MBA)]/Fe_3O_4/DES.

3.2. FTIR Spectra

Figure 4, shows the wide envelope at 3430 cm^{-1} is caused by overlapping O-H stretches of the PVA network and the hydroxylated choline cation, as well as N-H stretching of acrylamide's amide groups and urea's NH_2 moieties. Pure PVA films exhibit an -OH stretching vibration in the range of 3300-3500 cm^{-1} attributable to strong hydrogen bonding

between neighboring chains. Acrylamide hydrogels show a comparable N-H-stretch band at 3430 cm^{-1} for amide units. In a ChCl-urea DES, N-H stretches shift and expand due to significant H-bond formation between urea's NH_2 and chloride anions (and residual water), resulting in sub-bands at ~3400 and ~3310 cm^{-1}. The lower adsorption as 2944 and 2860 cm^{-1} correspond to aliphatic C-H stretches of PVA's -CH_2- backbone and methylene groups in MBA and acrylamide. PVA normally displays CH_2 stretches approximately 2900-2800 cm^{-1}. The imide I region in 1663 cm^{-1} corresponds to C=O stretching of the acrylamide units and the N, N′-methylenebisacrylamide cross-linking agent. The peak around 1660-1640 cm^{-1} is frequently encountered in polyacrylamide (PA nets). Imide II group, situated on 1600 cm^{-1}, results from N-H bending and C-N stretching in the same amide links. CH_2 scissoring and CH_3 bending in (ChCl) provide moderate intensity characteristics in the 1500-1400 cm^{-1} range, suggesting the existence of DES components [21]. A determined C-O stretching vibration of the PVA alcohol groups at 1099 cm^{-1} supports the network's unbroken poly(vinyl alcohol) backbone[23]. Residual sulfate species originating from the potassium persulfate (KPS) initiator give rise to two weaker peaks at 1117 cm^{-1} and 615 cm^{-1}. Corresponds to the asymmetric $V_3SO_4^{2-}$ stretch, while the latter is the bending ν_4 SO_4^{2-} mode, both vibrational modes are well-documented in FT-IR investigations of sulfate salts. Finally, the definite Fe-O stretch of magnetite occurs at 580 cm^{-1} (sometimes moved slightly lower to ~548 cm^{-1} in KBr pellets), unmistakably indicating Fe_3O_4 nanoparticles contained inside the polymer matrix [24].

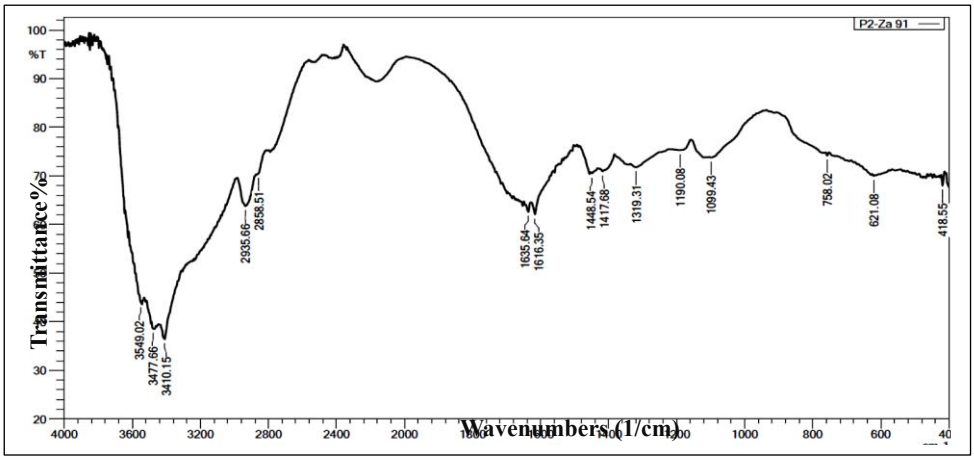

Figure 4:FTIR of [PVA-g-P (AAm-co-MBA)]/Fe_3O_4/DES

3.3. FESEM

As shown in Figure 5, the FESEM image exhibits a three-dimensional network with high porosity and interconnectivity, morphological features characteristic of hydrogels synthesized via free radical polymerization. The combination of acrylamide and MBA creates a crosslinked polyacrylamide matrix, whilst PVA leads to the production of a semi-crystalline structure, which improves the hydrogel's mechanical characteristics. The inclusion of urea and choline chloride (creating a DES) serves as a plasticizer, breaking down hydrogen bonds among PVA chains and increasing porosity and flexibility in the hydrogel network [25]. The FESEM picture shows embedded Fe_3O_4 nanoparticles as discrete bright spots inside the hydrogel matrix. These nanoparticles are evenly disseminated, showing that they were successfully incorporated throughout the polymerization process. Their presence gives the hydrogel magnetic reactivity, making it ideal for applications such as targeted medication delivery and magnetic separation [26]. The surface morphology is rough with linked pores, indicating that MBA has effectively assisted crosslinking. The polymerization process is

initiated by KPS, which ensures crosslinking. The presence of DES components (urea and choline chloride) alters the microstructure, resulting in increased swelling and mechanical strength.

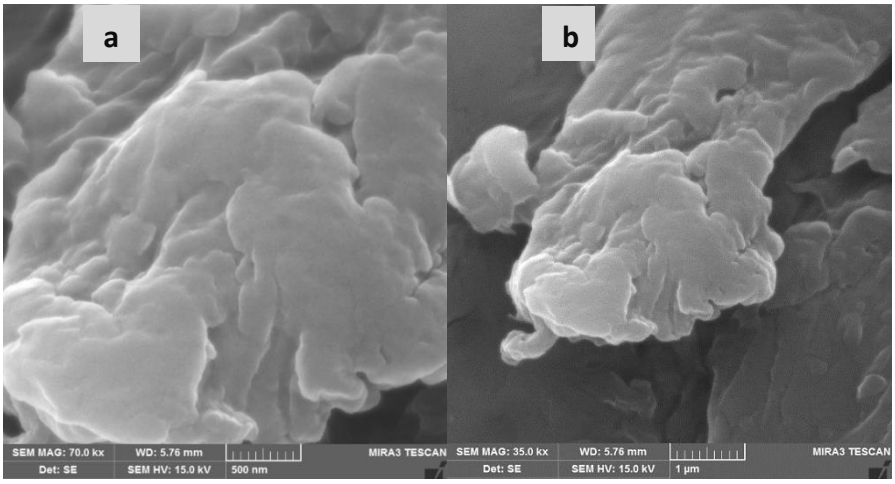

Figure 5: (a) FESEM picture of [PVA-g-P (AAm-co-MBA)]/Fe_3O_4/ DES Scale bar: 1 µm. (b) FESEM picture of [PVA-g-P (AAm-co-MBA)]/Fe_3O_4/ DES Scale bar: 500 nm.

4. Adsorption study

4.1. Adsorbent weight

Surface area plays a significant role in adsorption, As shown in Figure in Figure 6, the mass of [PVA-g-P (AAm-co-MBA)]/Fe_3O_4/DES varied from 0.01 to 0.1 g to study the effect on dye adsorbed. The initial dye concentration was maintained at 15 ppm, selected to ensure optimal absorbance according to Berlambert law, temperature was adjusted to 25°C, the time is 60 min and pH=6. Elimination percentages range between 33.3% and 68.3%. Figure 7, shows the increases in removal of dye rate associated with a comparable increase. The experiment showed that increasing the adsorbent weight from 0.01 g to 0.1 g improved dye removal from 33.3% to 68.3% because of the increased availability of active sites. The ideal adsorbent dosage is 0.1 g, as it offers enough surface area for efficient adsorption.

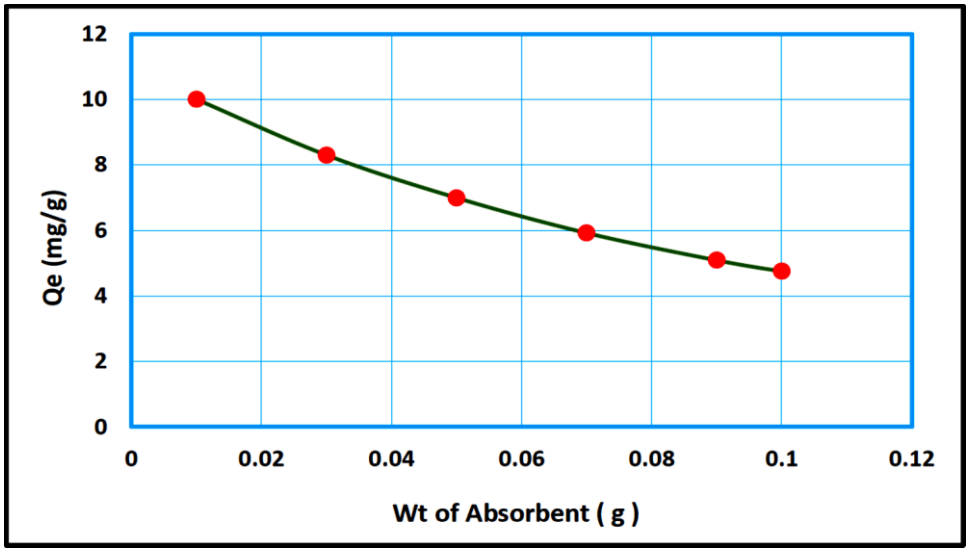

Figure 6: Effect of weight [PVA-g-P (AAm-co-MBA)]/Fe_3O_4/ DES on RB dye adsorption

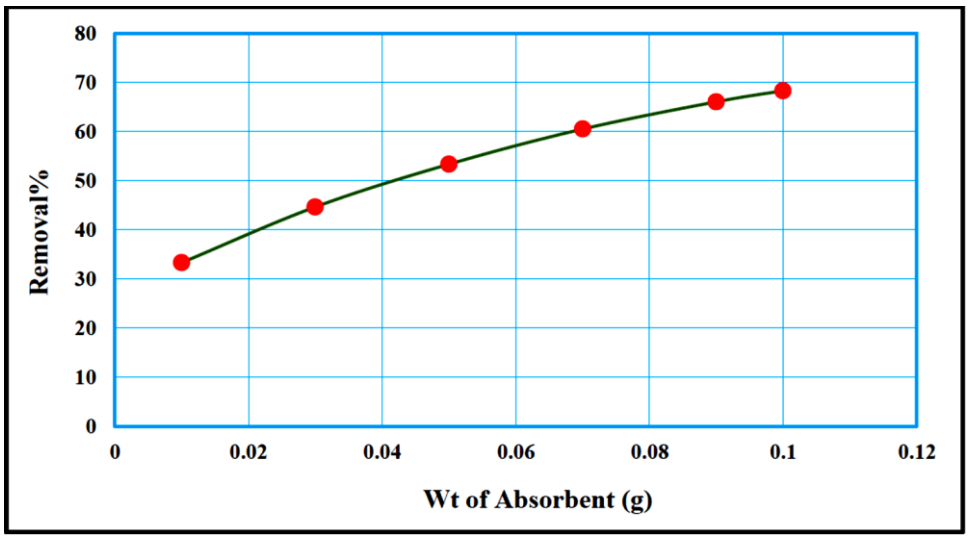

Figure 7: Removal % of RB

Increasing the adsorbent weight from 0.01 to 0.1 g increased the removal % owing to the increased availability of active sites. But the adsorption capacity per gram (q_e) was reduced due to site underutilization and particle aggregation. This is a prevalent and scientifically supported behavior.

4.2. Effect of RB contact time.

Figure 8, presents the adsorption equilibrium time for Rhodamine B dye evaluated at an initial a concentration of 15 ppm, and an adsorbent weight of 0.01 at temp 25°C, with a pH 6, across a varying contact times range from 1-90 minutes. Conclusions revealed a rapid adsorption rate during the initial phase, which is due to the elevated level specific surface area of the [PVA-g-P (AAm-co-MBA)]/Fe_3O_4/DES of 0.01g nanocomposite, offering numerous active sites for dye molecule interaction. The presence of oxygen-containing functional groups on the adsorbent surface significantly improves the adsorption kinetics in the first phase by offering active sites for fast interaction with Rhodamine B molecules [27]. Equilibrium was attained approximately at 60 min, which is Qe (60 min) = 11.0 $mg \cdot g^{-1}$.

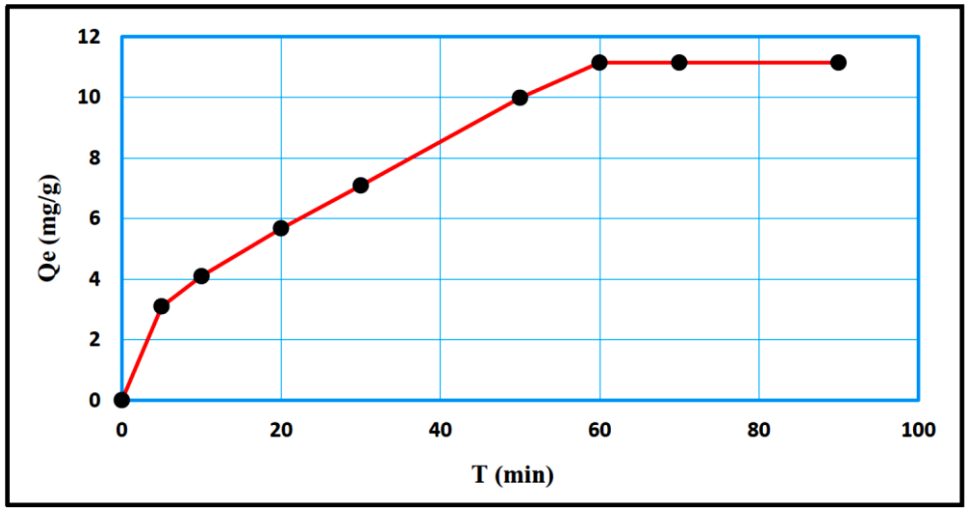

Figure 8: Effect of contact time of RB.

4.3. Effect of ionic strength

The level of ionization of the solution has a considerable impact on adsorption behavior, since it can affect how the molecular dyes react with the adsorbent surface. Variations in ionic strength, depending on the composition and valence of the ions present, can either boost or reduce adsorption efficiency. This study used 0.001, 0.01, 0.02, 0.03, 0.04, and 0.05 g of sodium chloride (NaCl) and calcium carbonate ($CaCO_3$) to test how ionic strength affects the adsorption of Rhodamine B (RB) dye. To identify the best adsorption conditions for both salts, critical factors such as temperature, adsorbent dose, surface loading, pH, and contact duration were evaluated thoroughly. Figure 9, shows the findings that demonstrate the weight of salt content upon the dye adsorption process. The adsorbent's adsorption capability decreases significantly as a result concentration of (NaCl) increases. A decline is due to competitive interactions between Na^+ ions and dye molecules for active sites on the adsorbent surface. Because of their modest ionic radius, Na^+ ions compete for adsorption sites, limiting dye adsorption. Additionally, Cl^- anions can form weak complexes with dye molecules, reducing adsorption effectiveness. While increasing calcium carbonate ($CaCO_3$) concentrations improves adsorption efficiency. The restricted solubility of $CaCO_3$ favors dye adsorption, allowing more molecules to engage with accessible active sites and increasing adsorption capacity [28].

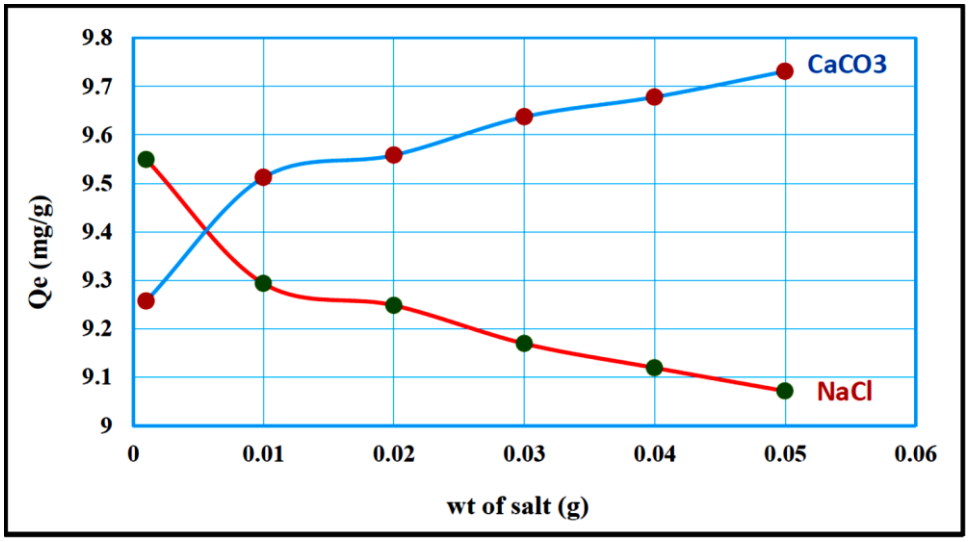

Figure 9: Effect of ionic strength.
[PVA-g-P (AAm-co-MBA)]/Fe_3O_4/ DES: 0.01 g, dye conc.: 15 ppm, temp.: 25 °C. Time: 60 min

4.4. Effect of pH

The adsorption process is heavily reliant on the management of the adsorbent's surface charge, the ionized state of dye molecules, as the separation behavior for functional categories on busy sites, all of which are greatly impacted by solution pH. Experiments were carried out at pH levels of 4, 6, 8, 10, and 12, as shown in figure 10, the results show that increasing the pH increases the amount of adsorbate until we reach pH=6, at which point we get the maximum amount of adsorbate due to increased dissociation at active site, positively change molecules of dye react more strongly with the negative charged adsorbent surfaces. This leads to a higher ability to absorb. But, as pH increases, the surface charge of the adsorbent becomes more negative or neutral, reducing electrostatic attraction and potentially causing repulsive interactions. Adsorption decreases at elevated pH levels due to the excessive negative charge on the surface repelling the positively charged Rhodamine B

molecules. So, higher pH values lower dye adsorption due to decreased surface charge density and increased dye repulsion [29].

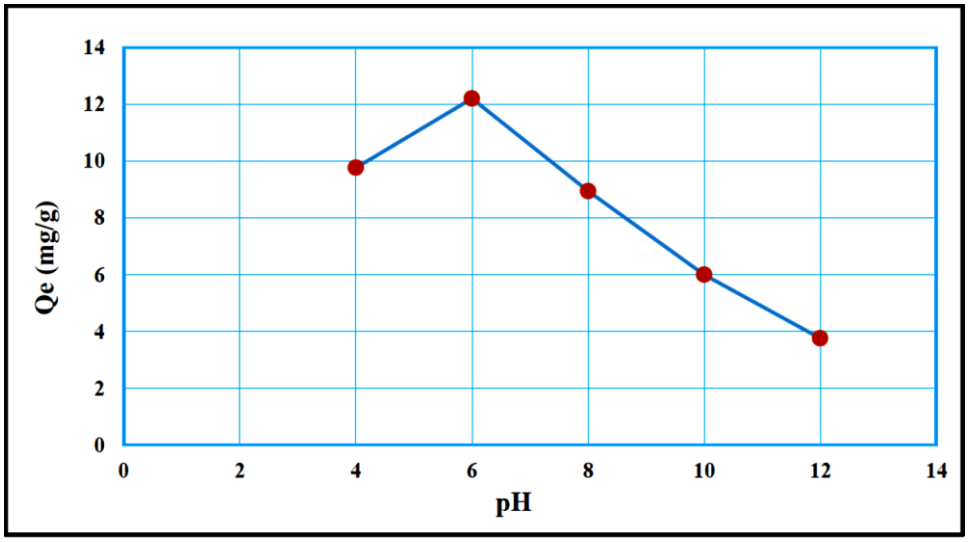

Figure 10: the impact of pH on elimination of RB dye.
[PVA-g-P (AAm-co-MBA)]/Fe_3O_4/ DES: 0.01 g, dye conc.: 15 ppm, temp.: 25 °C.

4.5. Effect of temperature

The colorant has been evaluated on the Nano composite surfaces at various temperature (25 to 55 ºC) this investigation identified whether the reaction was exothermic or endothermic. At pH= 6, different temperatures were used depending on surface fixing weight and adsorption period. Figure 11, demonstrates the efficacy of the adsorption process across a range of temperatures. Notably, the adsorption capacity for Rhodamine B dye decreases with increasing temperature, suggesting an exothermic adsorption mechanism. The principle of the van der Waals pressure exists among the molecules of color, with locations of activity diminishing as temperature rises, owing to increased molecular mobility, which influences the force that attracts particles to the outer layer [30]. Greater temperature produces more molecular mobility that increases the surface attraction to energetic locations in the outer layer. In rare situations, it might result in a reduction in the ability to adsorb. At temperatures rises entropy of the composite increases due to the random movement of adsorbed molecules on its surface. Pores also influence influences the procedure of adsorption mechanism when temperatures rises, the small pores enlarge increasing the outermost area accessible to connect to molecules that are adsorbed [31]. The enthalpy shift (ΔH) associated with the adsorption of Rhodamine B (RB) dye onto [PVA-g-P (AAm-co-MBA)]/Fe_3O_4/DES nanocomposite was evaluated by graphing the natural logarithm of the adsorption capacity (ln X_m) against the inverse temperature (1000/T), as shown in the figure 12, the linear connection shown allows for the computation of ΔH using Van't Hoff equations. A negative enthalpy value (ΔH^0 = -6.837 kJ/mol) suggests the method of adsorption mechanism is exothermic.

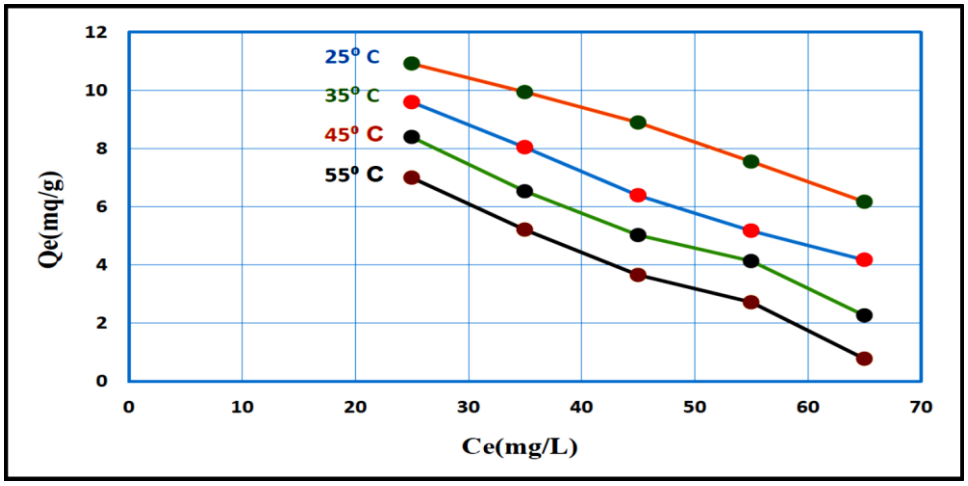

Figure 11: Effects of temperature in elimination of RB dye PVA-g-P (AAm-co-MBA)] /Fe_3O_4/ DES: 0.01 g, dye conc.: 15 ppm, temp.: 25-55 °C

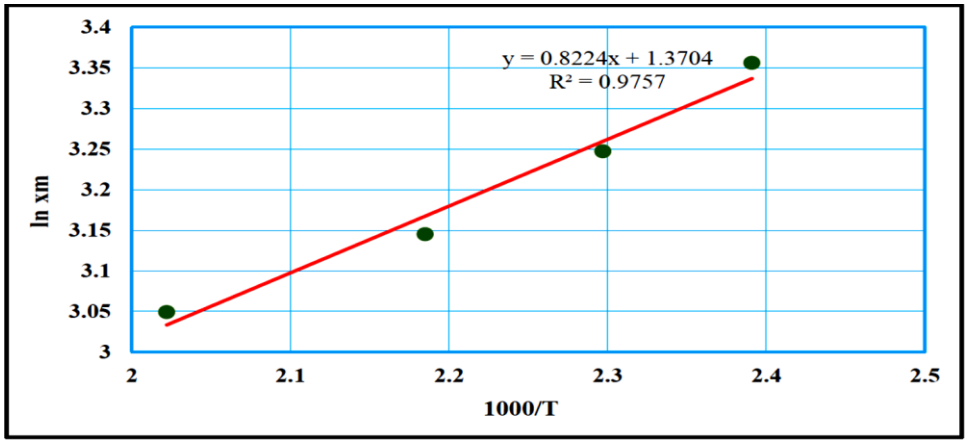

Figure 12: Adsorption of RB dye to the external layer of adsorbed *[PVA-g-P (AAm-co-MBA)]/Fe_3O_4/DES*

5. Adsorption Isotherms

Figures 13, 14, and 15, show Langmuir, Freundlich and Temkin isotherm, Both the Langmuir and Freundlich isotherm models were applied to interpret the adsorption process. The high correlation coefficients (R^2 values close to 1) from the linear graphs show that these models accurately explain how the dye is adsorbed, emphasizing that the composite material is well-suited for removing dye [32].

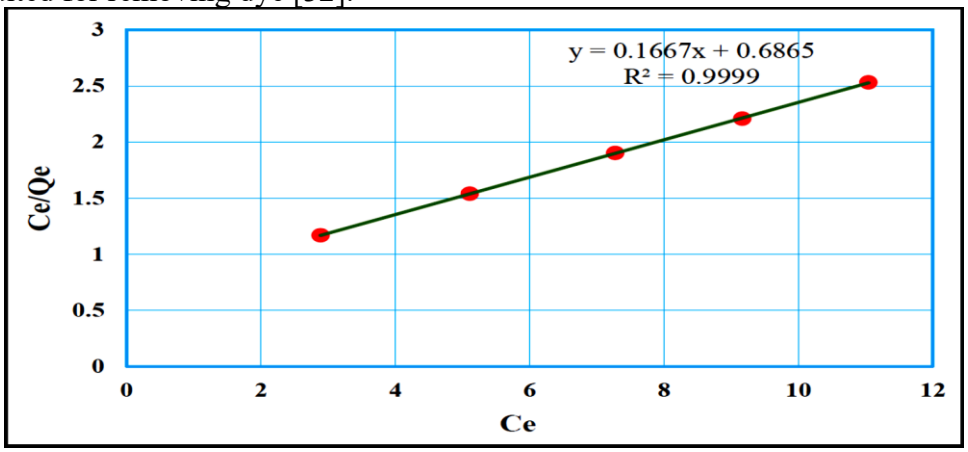

Figure 13: Langmuir isotherm.

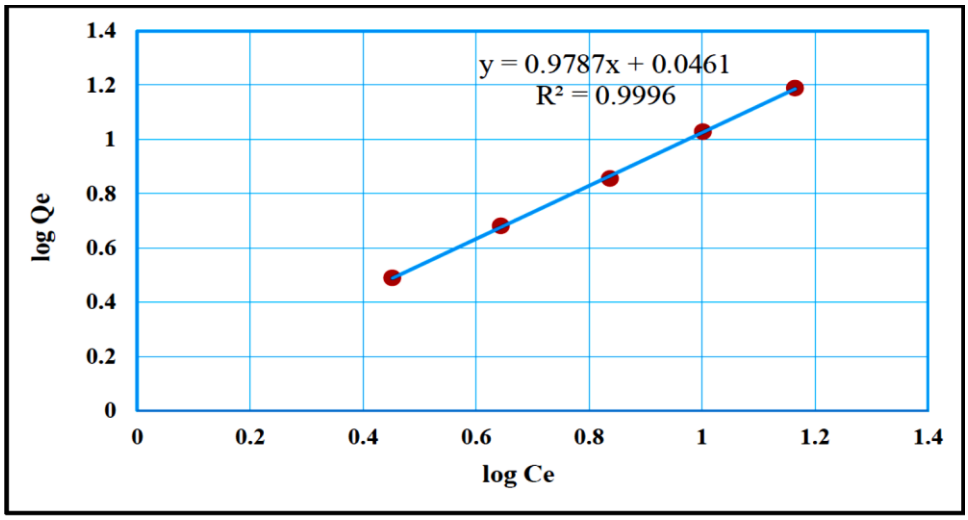

Figure 14: Freundlich isotherm.

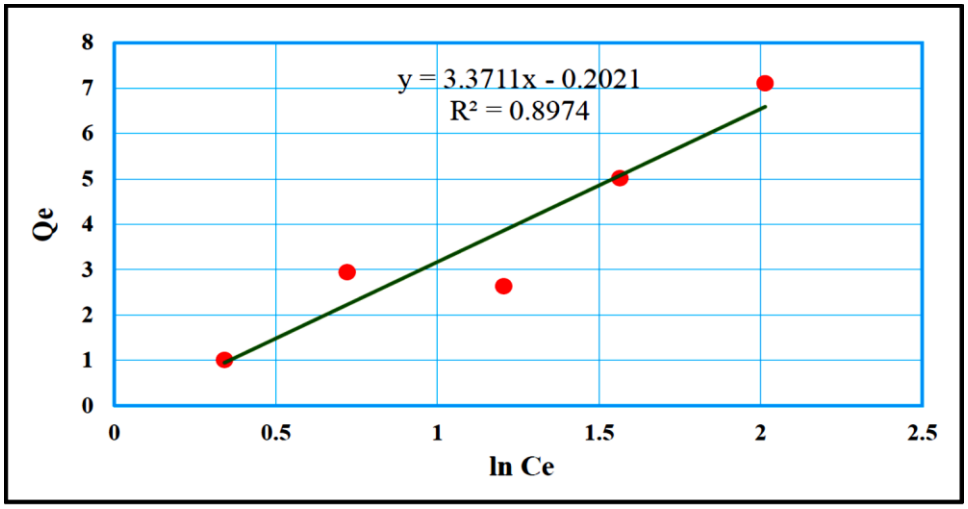

Figure 15: Temkin isotherm.

In Table 1 the Langmuir isotherm model exhibited an excellent fit to the experimental (R^2 = 0.9999), indicating that Rhodamine B attaches to the composite surface in a single layer on a consistent adsorbent surface. The highest amount that can be absorbed (Q_m) was 6.00 mg/g, and the Langmuir constant (K^L = 0.243 L/mg) shows that there is a moderate attraction between the dye molecules and the active sites on the adsorbent. In contrast, the Freundlich model showed a strong fit (R^2 = 0.9996), indicating surface heterogeneity and the possibility of multilayer adsorption. The Freundlich constant (n = 1.0217) is within the favorable adsorption range (1 < n < 10), indicating a spontaneous and advantageous adsorption process. The K_F value of 1.11 indicates a modest adsorption intensity on the heterogeneous surface. The Temkin model exhibited a lower correlation coefficient (R^2 = 0.8974), indicating a less precise depiction of the system in comparison to alternative models. The Temkin constants (b = 3.3711 J/mol and K_T = 1.0617 L/g), suggest that the heat of adsorption decreases slightly with an increase in surface area, indicating that the adsorption process is mainly physical.

Table 1: Adsorption isotherms constants

Dye	Langmuir Equation			Freundlich Equation			Temkin Equation		
	K_L	Q_m	R^2	K_F	n	R^2	K_T	B	R^2
Rhodamine B	0.243	6.00	0.9999	1.11	1.0217	0.9996	-1.0617	3.3711	0.8974

6. Adsorption Kinetics.

Kinetics analysis was conducted to evaluate the adsorption techniques duration and related influence on the adsorption capability. The dye solution was subjected to optimal experimental conditions, including temperature, pH and surface loading. Kinetic models were used on the experimental data to characterize the adsorption behavior, taking into consideration solid-liquid interactions. Figures 16 and 17 show the adsorption kinetics models with highest correlation, $R^2 = 0.9999$. This means that the pseudo-second-order kinetics model best explains how rhodamine B (RB) dye sticks to the composite surface, mainly through physical adsorption as presented shown in Table 2.

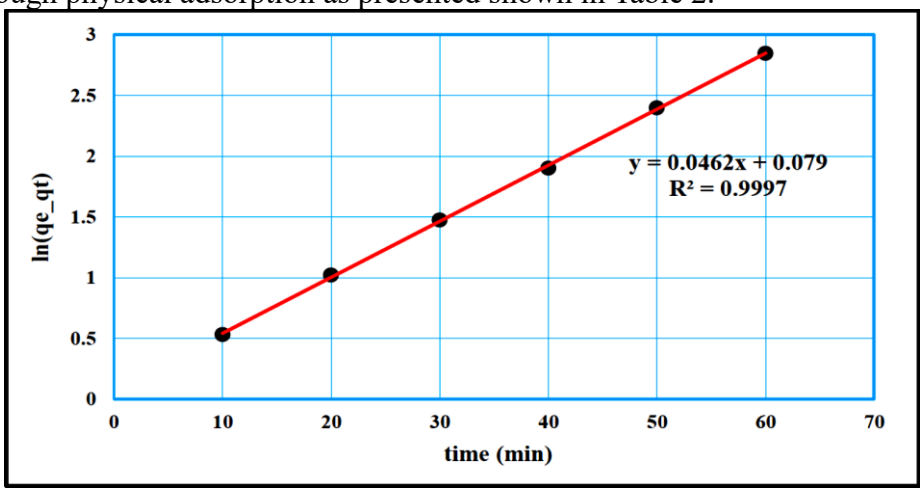

Figure 16: Pseudo first order model to RB color adsorption *[PVA-g-P (AAm-co-MBA)]/Fe_3O_4/ DES: 0.01 g, dye conc.: 15 ppm, temp.: 25 °C, pH: 6*

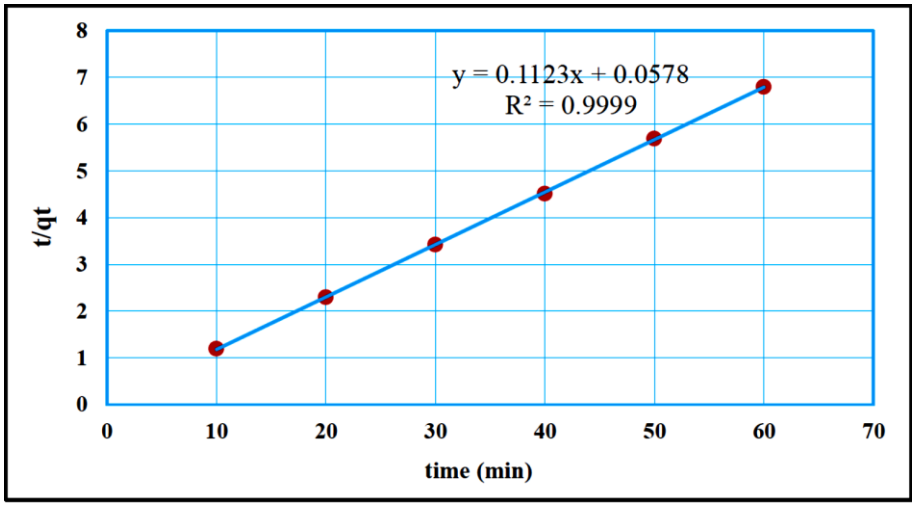

Figure 17: Pseudo second order model to RB color adsorption [PVA-g-P (AAm-co-MBA)]/Fe_3O_4/ DES: 0.01 g, dye conc.: 15 ppm, temp.: 25 °C, pH: 6

Table 2: Kinetic Parameters of Rhodamine B Adsorption onto the Composite Surface Based on Pseudo-First-Order and Pseudo-Second-Order Models.

Kinetic model	q_{exp} (mg/g)	q_{cal} (mg/g)	Rate constant	R^2
Pseudo-first-order	5.80	4.92	k_1=0.021 min^{-1}	0.9997
Pseudo-second-order	5.80	5.81	k_2=0.095 $g \cdot mg^{-1} \cdot min^{-1}$	0.9999

The adsorption results conform to the pseudo-second-order kinetic model with a strong correlation (R^2 = 0.9999). The computed enthalpy change ($\Delta H°$ = –6.837 kJ/mol) indicates a physical adsorption mechanism. Physisorption is generally linked to weak van der Waals interactions and little energy changes. Despite the kinetic compatibility, the low $\Delta H°$ value precludes chemisorption. Consequently, the adsorption of Rhodamine B on the composite surface is mostly governed by physisorption.

Conclusion

This study developed a novel magnetic polymeric composite, [PVA-g-P (AAm-co-MBA)]/Fe_3O_4/DES, synthesized from polyvinyl alcohol (PVA), acrylamide, N, N′-methylenebisacrylamide (MBA), Fe_3O_4 nanoparticles, and DES consists of choline chloride and urea. XRD, FTIR, and FESEM analysis validated the amorphous structure, the existence of functional groups, and the homogeneous distribution of magnetic nanoparticles inside the hydrogel matrix. Under a variety of experimental circumstances, the composite demonstrated efficient adsorption of Rhodamine B (RB). Adsorption was considerably affected by pH, contact duration, temperature, ionic strength, and adsorbent dose. The process had pseudo-second order kinetic, which indicated physical adsorption, and the Langmuir isotherm model best fitted the adsorption mechanism. Implying multilayer adsorption on a heterogeneous surface. Thermodynamic investigation showed that the adsorption was exothermic, with a negative $\Delta H°$ indicating a physical contact between the dye and composite, which is aided by its magnetic characteristics, which allow for simple separation and recovery. The [PVA-g-P (AAm-co-MBA)]/Fe_3O_4/DES composite is a promising, environmentally acceptable, and cost-effective adsorbent for removing hazardous dyes from aqueous media. It is a feasible contender for practical wastewater treatment applications.

Conflicts of Interests.

The writers report that there are no problems with interests linked to the study in question. Additionally, the writers do not have significant financial or other information to declare.

The acknowledgment.

The academics express their respective positions with heartfelt appreciation, thank you to the College of Sciences / the University of Al-Qadisiyah to feed assisting in finishing this task.

References

[1] C. Filote, A. Rosca, R. M. Hlihor, P. Cozma, I. M. Simion, M. Apostol, and M. Gavrilescu, “Sustainable application of biosorption and bioaccumulation of persistent pollutants in wastewater treatment: Current practice,” *Processes*, vol. 9, no. 10, p. 1696, 2021.

[2] M. C. Nayak, A. M. Isloor, B. Lakshmi, H. M. Marwani, and I. Khan, “Polyphenylsulfone/multiwalled carbon nanotubes mixed ultrafiltration membranes:

Fabrication, characterization and removal of heavy metals Pb^{2+}, Hg^{2+}, and Cd^{2+} from aqueous solutions," *Arabian Journal of Chemistry*, vol. 13, no. 3, pp. 4661–4672, 2020.

[3] A. V. Baskar, N. Bolan, S. Hoang, P. Sooriyakumar, M. G. Kumar, L. S. Singh, T. Jasemizad, L. P. Padhye, G. Singh, A. Vinu, B. Sarkar, M. B. Kirkham, J. Rinklebe, S. Wang, H. Wang, R. Balasubramanian, and K. H. M. Siddique, "Recovery, regeneration and sustainable management of spent adsorbents from wastewater treatment streams: A review," *Science of the Total Environment*, vol. 822, p. 153555, 2022.

[4] R. Ahmad and K. Ansari, "Chemically treated Lawsonia inermis seeds powder (CTLISP): An eco-friendly adsorbent for the removal of brilliant green dye from aqueous solution," *Groundwater for Sustainable Development*, vol. 11, p. 100417, 2020.

[5] T. Bayram, S. Bucak, and D. Ozturk, "BR13 dye removal using sodium dodecyl sulfate modified montmorillonite: Equilibrium, thermodynamic, kinetic and reusability studies," *Chemical Engineering and Processing: Process Intensification*, vol. 158, p. 108186, 2020.

[6] A. C. Fröhlich, R. Ocampo-Pérez, V. Diaz-Blancas, N. P. G. Salau, and G. L. Dotto, "Three-dimensional mass transfer modeling of ibuprofen adsorption on activated carbon prepared by sonication," *Chemical Engineering Journal*, vol. 341, pp. 65–74, 2018.

[7] M. Bartoli, M. Giorcelli, P. Jagdale, M. Rovere, and A. Tagliaferro, "A review of non-soil biochar applications," *Materials (Basel)*, vol. 13, no. 2, p. 261, 2020.

[8] S. S. Imam and H. F. Babamale, "A short review on the removal of rhodamine B dye using agricultural waste-based adsorbents," *Asian Journal of Chemical Sciences*, vol. 7, no. 1, pp. 25–37, 2020.

[9] P. O. Oladoye, M. Kadhom, I. Khan, K. H. H. Aziz, and Y. A. Alli, "Advancements in adsorption and photodegradation technologies for Rhodamine B dye wastewater treatment: Fundamentals, applications, and future directions," *Green Chemical Engineering*, vol. 5, no. 4, pp. 440–460, 2024.

[10] Y. Jiang, A. Wu, L. Yang, J. Wu, Y. Liang, Z. Hu, and Y. Wang, "Composite hydrogels based on deep eutectic solvents and lysine for pressure sensors and adsorption of Fe^{3+}," *RSC Advances*, vol. 14, no. 35, pp. 25359–25368, 2024.

[11] M. M. Islam, M. Chakraborty, P. Pandya, A. Al Masum, N. Gupta, and S. Mukhopadhyay, "Binding of DNA with Rhodamine B: Spectroscopic and molecular modeling studies," *Dyes and Pigments*, vol. 99, no. 2, pp. 412–422, 2013.

[12] H. Sereshti, S. Semnani Jazani, N. Nouri, and G. Shams, "Dispersive liquid–liquid microextraction based on hydrophobic deep eutectic solvents: Application for tetracyclines monitoring in milk," *Microchemical Journal*, vol. 158, p. 105269, 2020, doi: 10.1016/j.microc.2020.105269.

[13] I. Scopus Database, "In competition for water: Hydrated choline chloride: urea vs choline acetate: urea deep eutectic solvents," *ACS Sustainable Chemistry & Engineering*, vol. 9, no. 36, pp. 12262–12273, 2021.

[14] E. L. Smith, A. P. Abbott, and K. S. Ryder, "Deep eutectic solvents (DESs) and their applications," *Chemical Reviews*, vol. 114, no. 21, pp. 11060–11082, 2014.

[15] B. B. Hansen, S. Spittle, B. Chen, D. Poe, Y. Zhang, K. M. Klein, A. Horton, L. Adhikari, T. Zelovich, B. W. Doherty, B. Gurkan, E. J. Maginn, A. Ragauskas, M. Dadmun, T. A. Zawodzinski, G. Baker, M. E. Tuckerman, R. F. Savinell, and J. R. Sangoro, "Deep eutectic solvents: A review of fundamentals and applications," *Chemical Reviews*, vol. 121, no. 3, pp. 1232–1285, 2020.

[16] M. Á. Aguirre and A. Canals, "Magnetic deep eutectic solvents in microextraction techniques," *Trends in Analytical Chemistry*, vol. 146, 2022, doi: 10.1016/j.trac.2021.116500.

[17] G. Shen and B. Andrioletti, "Choline chloride/urea deep eutectic solvents: A promising reaction medium for the synthesis of bio-based poly(hydroxyurethane)s," *Molecules*, vol. 27, no. 13, p. 4131, 2022.

[18] Z. H. Abd Al-khuder and F. F. Karam, "Synthesis and characterization of a quaternary composite based on RGO/MWCNTs/choline chloride+ malonic acid for methyl orange dye adsorption," *Results in Chemistry*, vol. 15, p. 102133, 2025.

[19] U. A. Edet and A. O. Ifelebuegu, "Kinetics, isotherms, and thermodynamic modeling of the adsorption of phosphates from model wastewater using recycled brick waste," *Processes*, vol. 8, no. 6, p. 665, 2020.

[20] B. Li, M. Zhou, A. Wu, H. Liu, L. Du, and L. Su, "Preparation of PVA/PVDF/PAM-U composite hydrogels by in situ polymerization of ternary DES and their properties study," *Journal of Materials Science*, vol. 59, no. 2, pp. 715–727, 2024.

[21] R. Singh, D. Pal, and S. Chattopadhyay, "Target-specific superparamagnetic hydrogel with excellent pH sensitivity and reversibility: A promising platform for biomedical applications," *ACS Omega*, vol. 5, no. 34, pp. 21768–21780, 2020.

[22] C. Wang, G. Sang, M. Yang, G. He, Y. Rong, and J. Yang, "Microstructural transition of poly(vinyl alcohol)-based aerogels in the presence of interpolymer complexes," *New Journal of Chemistry*, vol. 46, no. 1, pp. 110–123, 2022.

[23] B. Lesiak, N. Rangam, P. Jiricek, I. Gordeev, J. Tóth, L. Kövér, M. Mohai, and P. Borowicz, "Surface study of Fe_3O_4 nanoparticles functionalized with biocompatible adsorbed molecules," *Frontiers in Chemistry*, vol. 7, p. 642, 2019.

[24] S. Kumaraswamy and S. H. Mallaiah, "Swelling and mechanical properties of radiation crosslinked Au/PVA hydrogel nanocomposites," *Radiation Effects and Defects in Solids*, vol. 171, no. 11–12, pp. 869–878, 2016.

[25] W. A.-A. Sadik, A.-G. M. El-Demerdash, H. A. Gabre, and M. E.-S. Hamza, "Effective removal of malachite green dye by eco-friendly pectin-grafted poly(acrylamide-co-sodium acrylate) hydrogel from aqueous solutions," *Polymer Bulletin*, vol. 82, no. 1, pp. 281–311, 2025.

[26] A. A. Oyekanmi, A. Ahmad, K. Hossain, and M. Rafatullah, "Adsorption of Rhodamine B dye from aqueous solution onto acid treated banana peel: Response surface methodology, kinetics and isotherm studies," *PLoS ONE*, vol. 14, no. 5, p. e0216878, 2019.

[27] D. Wang, Y. Zhao, and Q. Jia, "Construction of magnetic sulfonic-functionalized hypercrosslinked polymers for efficient adsorption of azole fungicides from water," *Separation and Purification Technology*, vol. 354, p. 128810, 2025.

[28] J. Guo, L. Fu, R. Gao, Y. Zhang, C. Yin, and B. Xue, "Efficiency removal of rhodamine B by MoS_2/magnetic potato residues biochar: Performance and mechanism," *Industrial Crops and Products*, vol. 233, p. 121390, 2025.

[29] B. Kayranli, M. Bilen, I. Y. Seckin, T. Yilmaz, A. Dinc, F. Akkurt, and H. Simsek, "Peanut shell biochar for Rhodamine B removal: Efficiency, desorption, and reusability," *Chemosphere*, vol. 364, p. 143056, 2024.

[30] S. Deutz and A. Bardow, "Life-cycle assessment of an industrial direct air capture process based on temperature–vacuum swing adsorption," *Nature Energy*, vol. 6, no. 2, pp. 203–213, 2021.

[31] E. S. Alwan, F. F. Karam, and Z. M. Kadam, "Kinetics, isotherms and thermodynamics study of eosin yellow dye adsorption from aqueous solutions by MnO_2@rGO nanocomposite," *Bulletin of the Chemical Society of Ethiopia*, vol. 39, no. 6, pp. 1213–1226, 2025.